Criticality in the Crossed Andreev Reflection of a Quantum Hall Edge

Vladislav D. Kurilovich and Leonid I. Glazman
Department of Physics, Yale University, New Haven, Connecticut 06520, USA

(Received 8 October 2022; accepted 3 August 2023; published 12 September 2023)

We develop a theory of the nonlocal transport of two counterpropagating $\nu = 1$ quantum Hall edges coupled via a narrow disordered superconductor. Contrary to the predictions developed for the clean case, the edge states proximitized in this way do not turn into a topological superconductor. Instead, they are naturally tuned to the critical point between trivial and topological phases. This occurs due to the competition between tunneling processes with and without particle-hole conversion. The critical conductance is a random, sample-specific quantity with a zero average and unusual bias dependence. The negative values of conductance are relatively stable against variations of the carrier density, which may make the critical state appear as a topological one. Our results offer an interpretation of recent experiments [G.-H. Lee *et al.*, Nat. Phys. **13**, 693 (2017); O. Gül *et al.*, Phys. Rev. X **12**, 021057 (2022)].

DOI: 10.1103/PhysRevX.13.031027 Subject Areas: Condensed Matter Physics, Mesoscopics, Superconductivity

I. INTRODUCTION

Topological superconductivity provides a promising route to fault-tolerant quantum computing [1]. A one-dimensional topological superconductor hosts non-Abelian excitations at its ends, such as Majorana zero modes [2] or their fractional generalizations, i.e., parafermions [3,4]. The nonlocal character of these modes can be harnessed to store quantum information in a way inherently protected from decoherence. One can manipulate the protected information by braiding the zero modes [5] thanks to their non-Abelian exchange statistics.

There are many proposed implementations of a one-dimensional topological superconductor (see, e.g., Refs. [6–9]). A versatile platform that may host Majorana zero modes (or parafermions) is a hybrid quantum Hall-superconductor structure [3,10,11]. The basic idea behind it is to couple two counterpropagating quantum Hall edges via a conventional superconductor. If the width of the superconductor d is comparable to the coherence length ξ, then two electrons residing in different edges can transfer into the superconductor as a Cooper pair. This process can be viewed as a nonlocal counterpart of the Andreev reflection and is thus called a crossed Andreev reflection (CAR). CARs establish superconducting correlations between the edges. At filling $\nu = 1$, which we focus on, the induced pairing has the p-wave symmetry, as required for the topological superconductivity supporting Majorana zero modes. In fact, experiments on quantum transport in such setups [12,13] (as well as in the related ones [14,15]) have already started. This motivated many recent theoretical works [16–21].

A complication in reaching the topological phase arises due to the elastic cotunneling (EC) processes which compete with CAR [22,23]. In an EC event, a particle tunnels across the superconductor without a conversion to a hole (contrary to the CAR event). This amounts to an electron-backscattering process. A strong backscattering is detrimental for the topological phase [24].

The competition between the CAR and EC processes is sensitive to disorder. We note that only a superconductor with a high upper critical field H_{c2} is compatible with the quantum Hall effect. This dictates the use of "dirty" superconductors with the electron mean free path $l_{\mathrm{MFP}} \ll \xi$ [12,13]. Because of the spin polarization of the $\nu = 1$ state, a particular relation between the CAR and EC probabilities is determined by the strength of the spin-orbit interaction in the system. At weak spin-orbit interaction, CAR processes are largely inhibited and EC prevails. This brings the proximitized edge states into a trivial phase. The prevalence of EC over CAR cannot be overturned no matter how strong the spin-orbit coupling is. It means that the topological phase cannot be reached by coupling quantum Hall edges via a disordered superconductor. At best, the probability of CAR may approach the EC probability. As we show, this brings the system to a critical point of the transition between the trivial and topological phases. We mention in passing that the EC processes were overlooked in the theoretical analysis of Ref. [13], as well as in the subsequent works [18,19].

The critical point belongs to the infinite-randomness universality class [25]. Although many authors studied the

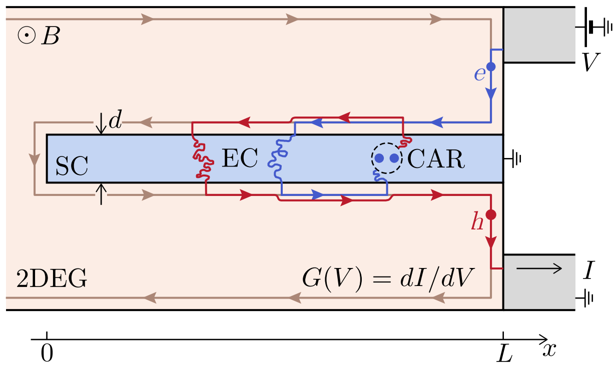

FIG. 1. Schematic layout of the considered setup. A narrow superconductor induces the proximity effect into two counterpropagating chiral edge states. Electrons are incident onto the superconductor from an upstream electrode biased by voltage V. Nonlocal conductance $G(V)$ is determined by the interference of elastic cotunneling and crossed Andreev reflection processes. These processes are random but are balanced statistically [see Eqs. (5)–(7)], which sets the proximitized edge states at the critical point between trivial and topological phases.

thermal transport of a superconductor in a critical state [26–28], the charge transport has attracted surprisingly little attention (with a notable exception of Ref. [29]). The conductance $G = dI/dV$ associated with the backscattered current I (see Fig. 1) is random. Its dependence on bias V is not well understood even at the smallest biases. Besides, little is known about the variations of the conductance with the device parameters such as the electron density. Such a parametric dependence is of direct relevance to the experiments, as the electron density is one of the simplest knobs which tunes the properties of the quantum Hall state. In this work, we address the bias and density dependence of the proximitized edge-states conductance.

At the critical point, the dependence of conductance on bias is a stochastic function alternating between positive and negative values. The pattern of these fluctuations is determined by a realization of the disorder in the superconductor. The criticality is reflected in the unusual logarithmic scaling of the differential conductance correlation function, which we quantify.

At any bias, the ensemble-averaged conductance is zero. The ensemble averaging can be achieved in a given device by varying its parameters, such as the electron density [30]. Interestingly, we find that the variation of the CAR amplitude happens at a much larger density scale than that of the EC amplitude. If—due to a statistical fluctuation—the former amplitude is relatively large, then the conductance may stay negative in a broad range of densities. This conclusion may help in interpreting recent experiments [12,13], in which a negative conductance stable to the variation of density was observed. Our theory shows that the observation of a negative conductance may be a facet of a critical state of proximitized edges and does not imply topological superconductivity.

II. MODEL

We consider two counterpropagating $\nu = 1$ quantum Hall edge states coupled through a narrow superconducting electrode; see Fig. 1. At low temperatures and bias, transport of the edge states can be described with the help of an effective low-energy Hamiltonian: $H_{\mathrm{eff}} = H_{\mathrm{QH}} + H_{\mathrm{prox}}$. The first term is the Hamiltonian of electron modes propagating along each of the edges:

$$H_{\mathrm{QH}} = \sum_{j=R,L} \int dx\, \psi_j^\dagger(x) v[-i\sigma_j \partial_x - k_\mu]\psi_j(x), \quad (1)$$

where $\psi_j(x)$ is the field operator of a right- ($j = R$) or left- ($j = L$) moving chiral electron $\sigma_{R/L} = \pm 1$, v is the edge-states Fermi velocity, and k_μ is their Fermi momentum.

The term H_{prox} describes the coupling between the edge states through the superconductor. We find it in the same way as in Ref. [17]: We start with the tunneling Hamiltonian H_{T} for the coupling of each of the edge states with the superconductor and then "integrate out" the superconductor's degrees of freedom. For electron energies $E \ll \Delta$ measured with respect to the Fermi level, the procedure results in

$$H_{\mathrm{prox}} = \sum_{i,j=R,L} \frac{t^2}{2} \int dx dx' \hat{\psi}_i^\dagger(x) \partial^2_{y_i y_j} \mathcal{G}(x, y_i; x', y_j) \hat{\psi}_j(x'). \quad (2)$$

Here, $\hat{\psi}_i(x) = (\psi_i(x), \psi_i^\dagger(x))^T$, $y_R = 0$, $y_L = d$, and d is the electrode width. Properties of the superconductor—such as its energy gap Δ and spin-orbit coupling in it—are encoded into the superconductor Green's function $\mathcal{G}$, which is a 2×2 matrix in the Nambu space. The normal derivatives are computed at the respective interfaces $y = 0, d$ [31,32]. t is the tunneling amplitude between each of the edge states and the superconductor.

We are interested in the differential conductance $G(V)$ of the three-terminal setup depicted in Fig. 1. A chiral electron incident on the superconducting electrode can be transmitted across it either as a particle or—if a crossed Andreev reflection happens—as a hole. By labeling the amplitudes of these processes at energy E as $A_{\mathrm{N}}(E)$ and $A_{\mathrm{A}}(E)$, respectively, we can express $G(V)$ at zero temperature as

$$G(V, T = 0) = G_Q(|A_{\mathrm{N}}(E)|^2 - |A_{\mathrm{A}}(E)|^2)|_{E=eV}, \quad (3)$$

where $G_Q = e^2/2\pi$ is the conductance quantum (we use units with $\hbar = 1$). One can view the two needed amplitudes as the entries of a scattering matrix $S(E)$ relating the incoming and outgoing electron and hole waves: $A_{\mathrm{N/A}}(E) \equiv S_{\mathrm{ee/he}}(E)$. Therefore, we need to find $S(E)$ to determine the conductance. A convenient way to do that is to first divide the electrode into a sequence of short elements (short enough to be treated perturbatively) and then track how $S(E)$ changes as we "build" the electrode by stacking the elements together.

III. SCATTERING OFF A SHORT ELEMENT

A single element acts as a bridge between the two chiral edges. As an electron traverses the bridge, it either turns into a hole (a CAR process) or remains an electron (an EC process). For a short element, we find the amplitudes of the two processes treating $H_{\rm prox}$ of Eq. (2) in the Born approximation. We obtain for CAR and EC amplitudes at the Fermi level, respectively,

$$\delta A_{\rm A} = \frac{t^2}{v}\int dx dx' e^{-ik_\mu(x'-x)}\partial^2_{yy'}\mathcal{G}^{\downarrow\uparrow}_{\rm he}(x,0;x',d), \qquad (4a)$$

$$\delta A_{\rm N} = \frac{t^2}{v}\int dx dx' e^{-ik_\mu(x'+x)}\partial^2_{yy'}\mathcal{G}^{\uparrow\uparrow}_{\rm ee}(x,0;x',d). \qquad (4b)$$

Here, $\mathcal{G}_{\rm he}$ and $\mathcal{G}_{\rm ee}$ are the anomalous and normal components of the Green's function of the superconductor [33]. The spin of a hole in a $\nu=1$ edge is opposite to that of an electron. Thus, for a CAR to happen the quasiparticle has to flip its spin upon traversing the element, as indicated by the $\uparrow\downarrow$ superscript in Eq. (4a). In our model, the spin-flip processes result from the spin-orbit scattering in the superconductor.

The Green's functions in Eqs. (4a) and (4b) describe the propagation of an electron wave across the superconducting element. Because of the diffraction of the wave on the impurities in the superconductor, the result of the wave propagation is stochastic. Therefore, $\mathcal{G}_{\rm ee/he}$ and $\delta A_{\rm A/N}$ are random quantities. We characterize their properties in an experimentally relevant regime of the electron mean free path $l_{\rm MFP} \ll d$ [12,13]. Under the latter condition, we can estimate $\langle\mathcal{G}_{\rm ee/he}\rangle \propto \exp(-d/2l_{\rm MFP}) \ll 1$, where $\langle\ldots\rangle$ denotes the average over the disorder configurations in the superconductor. In what follows, we neglect these exponentially small quantities and approximate $\langle\delta A_{\rm A}\rangle = \langle\delta A_{\rm N}\rangle = 0$.

Next, we find the variances $\langle|\delta A_{\rm A/N}|^2\rangle$ of the CAR and EC amplitudes. This requires averaging the product of the two Green's functions of the superconductor. Such an averaging can be performed by relating $\langle\mathcal{G}\times\mathcal{G}\rangle$ to the normal-state diffuson (see, e.g., [34]) via a standard procedure [35]. Focusing on the "dirty" superconductor and taking the spin-orbit scattering into account [36,37], we find for an element of length $\delta L \gg \xi$ and width $d \gg \xi$:

$$\langle|\delta A_{\rm A/N}|^2\rangle = \frac{\delta L}{l_{\rm A/N}}. \qquad (5)$$

The length scales $l_{\rm A}$ and $l_{\rm N}$ are given by [38]

$$\frac{1}{l_{\rm A/N}} = \frac{4\pi g^2}{G_Q\sigma}\sqrt{\frac{\pi\xi}{2d}}\left(e^{-d/\xi} \mp e^{-d/\xi^\star}\sqrt{\xi^\star/\xi}\right). \qquad (6)$$

Here, $g = 2\pi^2 G_Q p_F \nu_{\rm M}\nu_{\rm edge} t^2$ is the conductance per unit length of the interface between the chiral edge and the electrode in the normal state. The conductance depends on the Fermi momentum of the metal p_F and the density of states $\nu_{\rm M}$ in it, in addition to its dependence on the tunneling amplitude t and the density of states $\nu_{\rm edge} = 1/(2\pi v)$ at the edge. The dependence of $l_{\rm A/N}$ on the normal-state conductivity of the metal σ reflects the diffusive character of electron motion in the dirty superconductor. Finally, the information on the spin-orbit interaction is encoded in $\xi^\star = \xi/\sqrt{1+4/(3\tau_{\rm SO}\Delta)}$. Here, $\tau_{\rm SO}$ is the spin-orbit scattering time. Since a spin flip is needed for a CAR of a spin-polarized edge, $\delta A_{\rm A} = 0$ in the absence of spin-orbit scattering. This is why $1/l_{\rm A} = 0$ if $\xi = \xi^\star$.

Equations (5) and (6) show that, generically, $\langle|\delta A_{\rm A}|^2\rangle \leq \langle|\delta A_{\rm N}|^2\rangle$ [39]. The limit of strong spin-orbit coupling $\tau_{\rm SO}\Delta \ll 1$ is the most favorable one for the topological superconductivity. In this limit, the electron spin fully randomizes in the course of tunneling, which results in $\langle|\delta A_{\rm A}|^2\rangle = \langle|\delta A_{\rm N}|^2\rangle$. Equivalently,

$$l_{\rm A} = l_{\rm N} = 2l_0 \qquad (7)$$

(we introduce the factor of 2 for notational convenience). We demonstrate below that, in fact, the latter condition is *insufficient* to reach the topological phase; instead, it corresponds to a critical point of the transition between trivial and topological phases.

In addition to the nonlocal CAR and EC processes, an electron can return to the same edge after its excursion in the superconductor. This leads to accumulation of the forward-scattering phase $\delta\Theta_j$ $(j = R, L)$. We find $\langle\delta\Theta_j\rangle = 0$ and $\langle\delta\Theta_j^2\rangle = \delta L/l_{\rm F}$. The particular expression for $l_{\rm F}$ is inconsequential for our conclusions, and we relegate it to the Supplemental Material [38]. We note that the Pauli exclusion principle forbids an Andreev reflection within a single $\nu=1$ edge at the Fermi level. This is in contrast to the case of $\nu=2$ considered in Ref. [17].

Finally, only a type-II superconductor is compatible with the magnetic field required for reaching the quantum Hall state. The field may induce vortices, whose normal cores give rise to the nonvanishing density of states at the Fermi level in the superconductor [42]. As a result, a quasiparticle incident on the superconducting element can tunnel into it normally, irreversibly leaving the edges. We model such a quasiparticle loss phenomenologically by assigning to each element a loss probability $\delta p = 4\Gamma\delta L/v$ proportional to its length. Parameter Γ has a meaning of the rate at which the edge quasiparticles are lost.

IV. SCATTERING MATRIX OF A LONG ELECTRODE

An electron incident on a long ($L \gtrsim l_0$) superconducting electrode undergoes multiple CAR and EC processes.

In this case, one cannot directly apply the perturbation theory to find the scattering matrix. Instead, we break the electrode in a series of short elements labeled by their x coordinate and track how $S(E)$ evolves as we join the elements together. Equation (5) suggests to parametrize the scattering amplitudes of individual elements as $\delta A_{\mathrm{A/N}}(x) = \eta_{\mathrm{A/N}}(x) \times \sqrt{\delta L}/2$; similarly, we represent $\delta\Theta_j = \vartheta_j(x) \times \sqrt{\delta L}$. Random variables $\eta_m(x)$ $(m \in \{\mathrm{A}, \mathrm{N}\})$ and $\vartheta_j(x)$ $(j \in \{R, L\})$ are Gaussian, mutually independent, and uncorrelated for different x. Using Eq. (5) and the respective relation for the forward-scattering phase, we find for their correlators:

$$\langle \eta_m(x)\eta^\star_{m'}(x')\rangle = \frac{4\delta_{mm'}}{l_m}\delta(x-x') \tag{8}$$

and $\langle \vartheta_j(x)\vartheta_{j'}(x')\rangle = \delta_{jj'}\delta(x-x')/l_{\mathrm{F}}$ [45].

By evaluating the change of the scattering matrix upon an addition of a single short element to the electrode, we obtain the following equation for the evolution of $S(E)$ with x [38]:

$$i\frac{dS}{dx} = -\frac{2(E+i\Gamma)}{v}S + \mathcal{Q} + S\mathcal{Q}^\dagger S + S\mathcal{L} + \mathcal{R}S. \tag{9}$$

Here,

$$\mathcal{Q}(x) = \frac{i}{2}[\eta_{\mathrm{N}y}(x)\tau_0 - i\eta_{\mathrm{N}x}(x)\tau_z + \eta_{\mathrm{A}x}(x)\tau_y + \eta_{\mathrm{A}y}(x)\tau_x], \tag{10}$$

in which we introduce $\eta_{mx} \equiv \mathrm{Re}\,\eta_m$ and $\eta_{my} \equiv \mathrm{Im}\,\eta_m$; $\tau_{x,y,z}$ are the Pauli matrices in the Nambu space, and τ_0 is the identity matrix. $\mathcal{R}(x) = -\tau_z\vartheta_R(x)$ and $\mathcal{L}(x) = -\tau_z\vartheta_L(x)$. The initial condition is $S(E, x=0) = \tau_0$. A combination of terms $\mathcal{Q}$ and $S\mathcal{Q}^\dagger S$ describes the interference between the two paths in which an electron can tunnel from a right-moving edge into a left-moving one. The interference leads to the localization of wave functions of the edges. Note that the quasiparticle loss Γ plays the role of the level broadening.

V. CRITICALITY

We now apply Eq. (9) at $\Gamma = 0$ to reveal the critical behavior of the proximitized edges. We demonstrate the criticality by finding the low-energy density of states (DOS) $\nu(E)$ and conductance $G(E)$ in the limit of infinite length L [46]. To allow for small deviations from the critical point, we modify Eq. (7) by taking $l_{\mathrm{A}} = 2l_0(1+\lambda)$, $l_{\mathrm{N}} = 2l_0(1-\lambda)$ with $|\lambda| \ll 1$.

A particularly convenient parametrization of the S matrix for analyzing Eq. (9) is

$$S = \frac{1}{2}\begin{pmatrix} F_+(w_1,w_2)e^{i\alpha} & F_-(w_1,w_2)e^{i\phi} \\ F_-(w_1,w_2)e^{-i\phi} & F_+(w_1,w_2)e^{-i\alpha}\end{pmatrix}, \tag{11a}$$

$$F_\pm(w_1,w_2) = -\tanh w_1 + \frac{i}{\cosh w_1} \pm \mathrm{sign}(w_1-w_2)\left[-\tanh w_2 + \frac{i}{\cosh w_2}\right]. \tag{11b}$$

The variables $w_{1,2}$ here are defined in the interval $(-\infty, +\infty)$. Using this parametrization in Eq. (9), we obtain a system of equations governing the evolution of w_1, w_2, α, and ϕ:

$$\frac{dw_1}{dx} = \frac{2E}{v}\cosh w_1 + \eta_{\mathrm{N}x}\sin\alpha - \eta_{\mathrm{N}y}\cos\alpha + \eta_{\mathrm{A}x}\sin\phi - \eta_{\mathrm{A}y}\cos\phi, \tag{12a}$$

$$\frac{dw_2}{dx} = \frac{2E}{v}\cosh w_2 + (\eta_{\mathrm{N}x}\sin\alpha - \eta_{\mathrm{N}y}\cos\alpha - \eta_{\mathrm{A}x}\sin\phi + \eta_{\mathrm{A}y}\cos\phi)\mathrm{sign}(w_1-w_2), \tag{12b}$$

$$\frac{d\alpha}{dx} = \vartheta_R + \vartheta_L + q(w_1,w_2)(\eta_{\mathrm{N}x}\cos\alpha + \eta_{\mathrm{N}y}\sin\alpha), \tag{12c}$$

$$\frac{d\phi}{dx} = \vartheta_R - \vartheta_L - q(w_2,w_1)\mathrm{sign}(w_1-w_2) \times (\eta_{\mathrm{A}x}\cos\phi + \eta_{\mathrm{A}y}\sin\phi). \tag{12d}$$

Here we abbreviate $q(w_1,w_2) = \tanh(w_1+w_2/2)\Theta \times (w_1-w_2) + \coth(w_1-w_2/2)\Theta(w_2-w_1)$, with $\Theta(z)$ being the Heaviside step function. The initial conditions for Eqs. (12a)–(12d) are $w_1(x=0) = -\infty$, $w_2(0) - w_1(0) = \varepsilon$ [offset $\varepsilon > 0$ is needed to remove the ambiguity of $\mathrm{sign}(w_1-w_2)$ in Eq. (11b)], and $\alpha(0) = \phi(0) = 0$.

We will see momentarily that out of four variables, only w_1 and w_2 are important for finding $\nu(E)$ and $G(E)$. This makes it convenient to derive a simplified system of equations that would focus exclusively on variables w_1 and w_2. To do that, we first solve Eqs. (12c) and (12d) in a short interval dx, and then substitute the solutions into Eqs. (12a) and (12b). This leads to [38]

$$\frac{dw_i}{dx} = -\frac{\partial U(w_1,w_2)}{\partial w_i} + \tilde{\eta}_i(x). \tag{13}$$

This equation is similar to the Langevin equation for a Brownian particle moving in an external field. The noise terms $\tilde{\eta}_i(x)$ stem from $\eta_{\mathrm{N}}(x)$ and $\eta_{\mathrm{A}}(x)$ of Eq. (12); their correlators are $\langle\tilde{\eta}_i(x)\tilde{\eta}_j(x')\rangle = (1/l_0)\delta_{ij}\delta(x-x')$. The first term in Eq. (13) describes the drift of the $\vec{w}$ "particle" in an external field. The potential of the field is given by

$$U(w_1,w_2) = -\frac{2E}{v}(\sinh w_1 + \sinh w_2) - \frac{1}{l_0}\ln|\sinh w_1 - \sinh w_2| + \frac{\lambda}{l_0}(w_1-w_2). \tag{14}$$

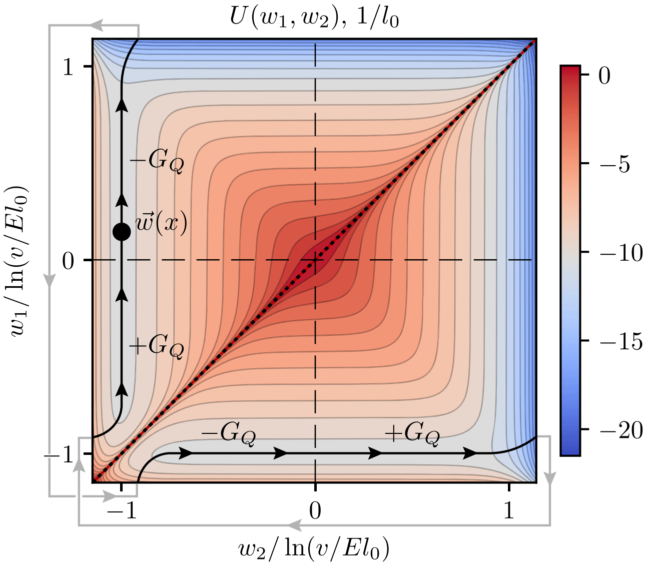

FIG. 2. Effective potential $U(w_1, w_2)$ for variables w_1, w_2 which parametrize the scattering matrix S [see Eq. (14)]. The potential landscape is plotted for $\ln(v/El_0) = 12$ at the critical point $\lambda = 0$. The motion of the $\vec{w}$ particle is cyclic (connected black and gray lines). It is confined to two nearly equipotential trenches: a vertical one at $w_2 = -\ln(v/El_0)$ and a horizontal one at $w_1 = -\ln(v/El_0)$. The low-energy conductance takes quantized values $\pm G_Q$ depending on the position of $\vec{w}(L)$ in the (w_1, w_2) plane.

The potential is plotted in Fig. 2. In the low-energy limit $E \ll v/l_0$, and for $|\lambda| \ll 1$, the dynamics of the $\vec{w}$ particle is confined to two elongated trenches of length $2\ln(v/El_0) \gg 1$. Both trenches end with a "cliff": The potential rapidly and boundlessly drops down for $w_{1,2} \gtrsim \ln(v/El_0)$ due to the first term in Eq. (14). The motion of the $\vec{w}$ particle is cyclical. In one part of the cycle, $\vec{w}$ moves along the vertical trench until it reaches the cliff. When it falls off the cliff, it reemerges on the opposite side of the (w_1, w_2) plane; see Fig. 2. After that, a complementary part of the cycle starts in which variables w_1 and w_2 trade places. The jump in one variable occurs at a fixed value of another variable, as required by the continuity of the S matrix as a function of x.

The conductance $G(E)$ is determined by the end point of the $\vec{w}$ particle's evolution. Using Eqs. (3) and (11), we can express $G(E)$ in terms of the values of w_1 and w_2 at $x = L$ as

$$G(E) = G_Q \mathrm{sign}[w_1(L) - w_2(L)] \tanh w_1(L) \tanh w_2(L). \tag{15}$$

In the low-energy limit, one can approximate $\tanh w_i(L)$ by $\mathrm{sign}\, w_i(L)$. Indeed, the two functions differ from each other only in a narrow interval of w_i near $w_i = 0$. The width of this interval is of the order of 1, which is much smaller than the lengths of the trenches $2\ln(v/El_0) \gg 1$ for the motion of the $\vec{w}$ particle. This shows that the low-energy conductance is quantized, $G(E) = \pm G_Q$; the accuracy of quantization is controlled by a small parameter $1/\ln(v/El_0) \ll 1$. The dependence of the quantized value of $G(E)$ on $\vec{w}(L)$ is illustrated in Fig. 2.

The integrated density of states $N(E) = \int_0^E dE' \nu(E')$ can also be related to the S matrix [47]:

$$N(E) = \frac{1}{L}\frac{1}{2\pi i} \ln \det S(E, L). \tag{16}$$

Because of the unitarity of the scattering matrix, $\det S = e^{i\beta}$. Equation (11) shows that the phase β winds by 2π every time the particle completes a full cycle in the (w_1, w_2) plane. Consequently, to find $N(E)$ we need to determine the number of cycles made by the particle per unit "time" x.

The potential U changes linearly along the trenches due to the third term in Eq. (14). If $\lambda > 0$, then the particle diffuses uphill along the vertical trench and downhill along the horizontal one. As a result, it spends the majority of time being trapped in the potential well near the point $[-\ln(v/El_0), -\ln(v/El_0)]$ on the vertical trench. In the limit $E \to 0$, the potential well becomes infinitely deep and, according to Eq. (15), the conductance distribution function approaches $P(G) = \delta(G - G_Q)$.

The configuration reverses for $\lambda < 0$ [48]. The trapping of the particle happens on a horizontal trench instead of a vertical one. This results in a perfect Andreev reflection at $E \to 0$, i.e., $P(G) = \delta(G + G_Q)$. The above distribution functions identify $\lambda > 0$ and $\lambda < 0$ as trivial and topological phases, respectively.

Because of the trapping, the particle completes a cycle in the (w_1, w_2) plane only by rare events of the overbarrier "thermal" activation allowed by the noise term in Eq. (13). The height of the barrier is $\Delta U = 2|\lambda| \ln(v/El_0)/l_0$, while the effective temperature equals $1/l_0$ [49]. Then, using Eq. (16), we can estimate $N(E) \propto \exp(-l_0 \Delta U) \propto E^{2|\lambda|}$, which yields

$$\nu(E) \propto \frac{1}{E^{1-2|\lambda|}} \tag{17}$$

for the DOS. The conclusions for $G(E)$ and $\nu(E)$ hold as long as the activation barrier is large, $\Delta U \gtrsim 1/l_0$, which translates to $E \lesssim (v/l_0)\exp(-c/|\lambda|)$ with $c \sim 1$. At higher energies, $G(E)$ and $\nu(E)$ behave in the same way as at the critical point, $\lambda = 0$. In fact, condition $\lambda = 0$ arises naturally in the limit of strong spin-orbit coupling; see Eq. (7) and the preceding discussion. Under this condition, the particle undergoes a free Brownian motion along the equipotential trenches. It completes a cycle in a "time" $\Delta x \sim l(E)$ with $l(E) = l_0 \ln^2(v/El_0)$. The length scale $l(E)$ plays the role of a correlation radius at a critical point at energy E. As a result, we find

$N(E) \sim 1/\Delta x \sim [l_0 \ln^2(v/El_0)]^{-1}$. Thus, the DOS $\nu(E) = \partial N(E)/\partial E$ has a Dyson singularity [50] at the Fermi level:

$$\nu(E) \propto \frac{1}{E \ln^3(v/El_0)}. \tag{18}$$

This singularity is indicative of the topological phase transition in one-dimensional superconductors [24,25].

The value of the conductance at the critical point is random and sample specific. It is determined by the end point of the particle's random walk along the equipotential trenches, as shown in Fig. 2. In the limit $E \to 0$, the conductance distribution function approaches $P(G) = [\delta(G - G_Q) + \delta(G + G_Q)]/2$. To understand this result, we note that the critical state can be pictured as an alternating sequence of trivial- and topological-phase domains [25] of a typical size $l(E)$. Conductance measured at bias $eV = E$ depends on the type of the domain adjacent to the superconductor's end. If this domain is topological, then the scattering of an incident electron happens similarly to that off a conventional Majorana wire, $G = -G_Q$ (we remind that G characterizes the backscattered current). In the opposite case, it is similar to the scattering off an insulator, $G = +G_Q$. The type of the end domain depends on disorder realization, but the two possibilities are equally probable reflecting the criticality.

VI. DIFFERENTIAL CONDUCTANCE AT THE CRITICAL POINT

To quantify the behavior of $G(E)$ at $\lambda = 0$, we find the conductance correlation function $\mathcal{C}_E(E_1, E_2) = \langle G(E_1)G(E_2)\rangle / \langle G^2 \rangle$ at $T = 0$. The conductance at energy E is determined by a disorder realization in a segment of the superconductor of size $l(E)$ adjacent to its end; the correlation radius $l(E)$ is the only relevant length scale at the critical point. In the spirit of the infinite-randomness model [51], we expect that the energy dependence of the conductance comes only from the respective dependence of $l(E)$. Thus, the dimensionless function $\mathcal{C}_E(E_1, E_2)$ must have a one-parameter scaling form:

$$\mathcal{C}_E(E_1, E_2) = \tilde{f}(l(E_1)/l(E_2)) = f\left(\frac{\ln \frac{1}{E_1}}{\ln \frac{1}{E_2}}\right) \tag{19}$$

(hereinafter, we suppress v/l_0 under the logarithms for brevity). Without loss of generality, we assume below that $0 < E_2 < E_1$, such that the argument of scaling function $f(x)$ satisfies $0 < x < 1$.

The form of $f(x)$ can be established analytically for $1 - x \ll 1$. To do that, we compare the results of the evolution of the $\vec{w}$ particles at two close energies E_1 and E_2. While the noise acting on $\vec{w}_{E_1}$ and $\vec{w}_{E_2}$ is the same [see Eq. (12)], the potential landscapes in which they move are different: The lengths of the respective trenches differ by a relative amount $1 - \ln(1/E_1)/\ln(1/E_2)$; see Eq. (14). The conductances $G(E_1)$ and $G(E_2)$ are opposite to each other if the two particles end up on different halves of the respective trenches; see inset of Fig. 3(b). Such configurations reduce the correlation function from unity. Let us consider a single cycle of motion of the $\vec{w}$ particles. $\vec{w}_{E_1}$ and $\vec{w}_{E_2}$ start their motion at the beginning of the respective trenches and move synchronously. However, they reach the middles of their trenches at different "times," as the trenches have different lengths. It takes a typical time $\Delta x \sim l(E)$ for a particle to reach the middle of the trench. At that time, the probability density to find the particle at distance δw from the beginning of the trench is given by the diffusion kernel $P(\delta w, \Delta x) = (\pi \Delta x/l_0)^{-1/2} \exp[-(\delta w^2/4\Delta x/l_0)]$. We can estimate $1 - \mathcal{C}_E(E_1, E_2)$ as the probability for two particles to be on different sides of the respective middle points:

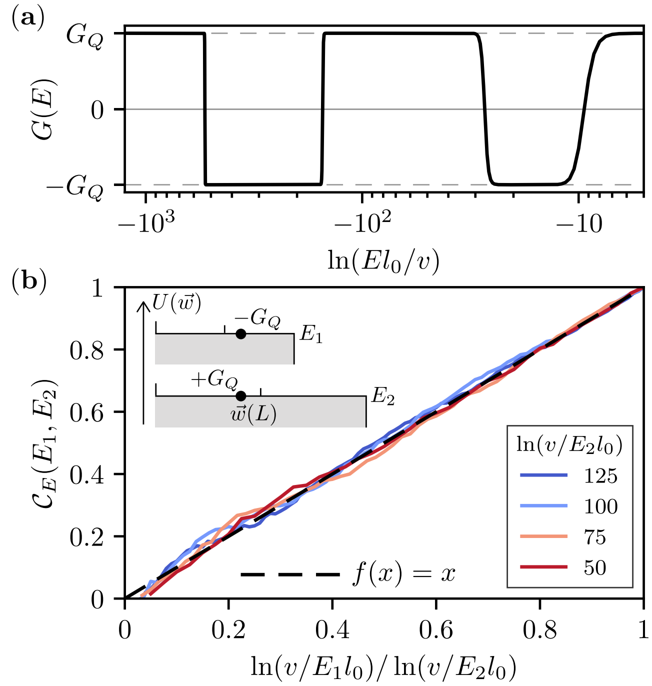

FIG. 3. Critical behavior of conductance $G(E)$. (a) At low energies, $G(E)$ switches stochastically between the quantized values $\pm G_Q$. Note that the scale is double logarithmic in E. To plot the curve, we numerically simulate the S-matrix evolution for $L = 9 \times 10^4 l_0$ and use Eq. (15). (b) Correlation function $\mathcal{C}_E(E_1, E_2)$ of the conductances at different energies (solid lines). $\mathcal{C}_E(E_1, E_2)$ is evaluated numerically; to perform the averaging over disorder realizations in the definition of $\mathcal{C}_E$, we compute $G(E)$ for 2500 samples [we use a version of Eq. (12) simplified in the low-energy limit to find $G(E)$; see Eq. (S44) of Ref. [38]]. The curves plotted for different $\ln(v/E_2 l_0)$ coincide with each other. This verifies scaling relation (19). Scaling function $f(x)$ is well approximated by $f(x) = x$ (dashed line). Inset: deviation of $\mathcal{C}_E(E_1, E_2)$ from unity stems from the configurations in which the $\vec{w}$ particles at energies E_1 and E_2 end their evolution on the opposite halves of the equipotential trenches.

$$1 - \mathcal{C}_E(E_1, E_2) \sim \int_0^{2\ln\frac{1}{E}} d(\delta w)\left[1 - \mathrm{sign}\left(\delta w - \ln\frac{1}{E_1}\right) \times \mathrm{sign}\left(\delta w - \ln\frac{1}{E_2}\right)\right] P(\delta w, \Delta x). \quad (20)$$

By estimating the integral, we find

$$1 - \mathcal{C}_E(E_1, E_2) \sim 1 - \frac{\ln\frac{1}{E_1}}{\ln\frac{1}{E_2}}, \quad (21)$$

i.e., $1 - f(x) \sim 1 - x$ for $1 - x \ll 1$.

For an arbitrary relation between E_1 and E_2, we find the correlation function numerically by simulating Eq. (12) (see Ref. [38] for details). The result of the simulation is presented in Fig. 3(b). Surprisingly, $f(x)$ appears to be well approximated by $f(x) = x$ in the whole interval $x \in [0, 1]$.

Finally, Fig. 3(a) demonstrates $G(E)$ for a particular realization of the disorder. At low energies, the values of the conductance stochastically alternate between $+G_Q$ and $-G_Q$. These changes are uniform in variable $\ln\,\ln(1/E)$; cf. Eq. (19). It means that the fluctuations of $G(E)$ become increasingly dense at $E \to 0$. At the lower end, the rapid fluctuations are cut off either by energy $E_L \sim (v/l_0) \times \exp(-\tilde{c}\sqrt{L/l_0})$ at which the correlation radius $l(E)$ becomes comparable to the system size L (with $\tilde{c} \sim 1$), or by the level broadening Γ induced by vortices.

The $\ln\,\ln E$ scale comes from the mechanism of the conductance variations. Upon the decrease of energy, $G(E)$ jumps from G_Q to $-G_Q$ every time a new energy level appears on the length scale $l(E) \sim l_0 \ln^2(1/E)$. The respective change of energy satisfies the condition $\nu(E)l(E)\delta E \sim 1$, which can be cast in the form $\delta[\ln\,\ln(1/E)] \sim 1$ with the help of Eq. (18) for the DOS. The emergence of the double-logarithmic scale was also noticed in Ref. [29].

VII. INFLUENCE OF VORTICES

So far, we have neglected the influence of vortices on the conductance. An incident electron may sink into the vortex core, thus dropping out of the backscattered current. Thus, vortices suppress the magnitude of G. To illustrate this effect, we find the distribution function $P(G)$ in the regime of strong absorption, $\Gamma \gg v/l_0$. In this regime, an incident electron undergoes at most a single EC or CAR process. This allows us to find the respective amplitudes perturbatively in $\eta_{\mathrm{A/N}}(x)$. Using Eq. (9), we obtain at $E \ll \Gamma$ [52]:

$$A_{\mathrm{A/N}} = -\frac{i}{2}\int_0^L dx e^{-\frac{2\Gamma}{v}(L-x)} \eta_{\mathrm{A/N}}(x). \quad (22)$$

The conductance distribution function can be expressed as $P(G) = \langle \delta(G - G_Q(|A_{\mathrm{N}}|^2 - |A_{\mathrm{A}}|^2)) \rangle$, where $\langle \ldots \rangle$ denotes the average over the realizations of $\eta_{\mathrm{A/N}}(x)$. Substituting

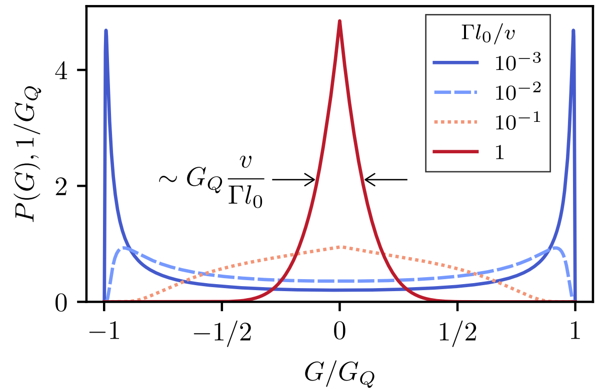

FIG. 4. Distribution function $P(G)$ of the zero-bias conductance in the presence of the quasiparticle absorption induced by the vortices. When the absorption is weak $\Gamma l_0/v \ll 1$, the conductance is close to one of the two quantized values $\pm G_Q$. Stronger absorption reduces the characteristic magnitude of G. For $\Gamma l_0/v \gtrsim 1$, the conductance is symmetrically distributed in a narrow interval around $G = 0$; see Eq. (23). An expression for $P(G)$ valid at arbitrary Γ is presented in the Supplemental Material [38].

Eq. (22) into this expression and using Eq. (8), we obtain at the critical point:

$$P(G) = \frac{1}{G_Q}\frac{4\Gamma l_0}{v}\exp\left[-\frac{8\Gamma l_0}{v}\frac{|G|}{G_Q}\right]. \quad (23)$$

The absorption renders the typical magnitude of the conductance small, $|G| \sim G_Q(v/\Gamma l_0) \ll G_Q$. This is in contrast to the case of $\Gamma = 0$, in which $G = \pm G_Q$. Importantly, $P(G)$ remains symmetric at all values of Γ reflecting the criticality. The crossover between a single-peak $P(G)$ at $\Gamma \gg v/l_0$ and its two-peak counterpart in the opposite limit is illustrated in Fig. 4. The regime of strong quasiparticle absorption may be relevant for the recent experiments [12,13], in which $|G| \ll G_Q$ was measured.

VIII. PARAMETRIC CORRELATIONS

In the conventional mesoscopic transport, there is no need to collect the data from an ensemble of devices to measure the statistics of the conductance fluctuations. The ensemble averaging can be achieved in a *single* sample by varying its parameters, such as the electron density [30,53,54]. This result is known as the ergodicity hypothesis.

The variation δn of the electron gas density changes the Fermi momentum of edge-states electrons by $\delta k_\mu = \delta n(\partial\mu/\partial n)/v$, where $\partial\mu/\partial n$ is the inverse compressibility of the quantum Hall state. The change of k_μ affects the phases of the EC amplitudes, $\eta_{\mathrm{N}}(x) \to \eta_{\mathrm{N}}(x)e^{-2i\delta k_\mu x}$; see Eq. (4b). However, the CAR amplitudes remain approximately intact, $\eta_{\mathrm{A}}(x) \to \eta_{\mathrm{A}}(x)$; see Eq. (4). Because of this, the ergodicity may appear to *break down* for the proximitized counterpropagating edges. The variation of $\eta_{\mathrm{A}}(x)$

with k_μ happens due to subtle effects only, such as the nonlocal character of the electron tunneling between the edges. Indeed, the x coordinate of a tunneling electron may change by an amount of the order of $\sqrt{\xi d}$, which sets a scale of $1/\sqrt{\xi d}$ for the variation of $\eta_A(x)$ with k_μ.

To demonstrate the existence of two scales for the density variation, we compute the correlation function $\mathcal{C}_n(\delta n) = \langle G(n+\delta n)G(n)\rangle/\langle G^2\rangle$, focusing on the regime of strong quasiparticle absorption, $\Gamma \gg v/l_0$. In this regime, one can use the perturbative expressions of Eq. (22) to find $\mathcal{C}_n(\delta n)$. Substituting them in Eq. (3) and using Eq. (8) (together with its counterpart for the amplitude correlations at different k_μ [38]), we obtain

$$\mathcal{C}_n(\delta n) = \frac{1}{2}\exp\left[-\left(\frac{\delta n}{n_{c,A}}\right)^2\right] + \frac{1}{2}\frac{1}{1+(\delta n/n_{c,N})^2}. \quad (24)$$

Here, $n_{c,N} = 2\Gamma(\partial n/\partial\mu)$ and $n_{c,A} = (v/\sqrt{\xi d})(\partial n/\partial\mu)$ are the two scales of the variation of G with n. We see that the latter of the two scales diverges at $\sqrt{\xi d} \to 0$ leading to the saturation of $\mathcal{C}_n(\delta n)$ at $\delta n \gg n_{c,N}$ and creating an appearance that the ergodicity breaks down.

The saturation of $\mathcal{C}_n(\delta n)$ persists at smaller values of Γ. In the limit $\Gamma \to 0$, the parameter Γ in the scale $n_{c,N}$ is replaced by v/l_0. To see the saturation at $\Gamma = 0$, we find $\mathcal{C}_n(\delta n)$ by numerically simulating Eq. (12). The result of the simulation is presented in Fig. 5 for different values of E. We see that $\mathcal{C}_n(\delta n)$ saturates at $\simeq 0.31$ independent of E. This can be explained by analyzing the Fokker-Planck equation for the joint distribution function of the $\vec{w}$ variables at two values of density separated by $\delta n \gg n_{c,N}$ [38]. In this limit, the Fokker-Planck equation acquires an elliptic form. The independence of $\mathcal{C}_n(\delta n)$ of E stems from its scaling properties.

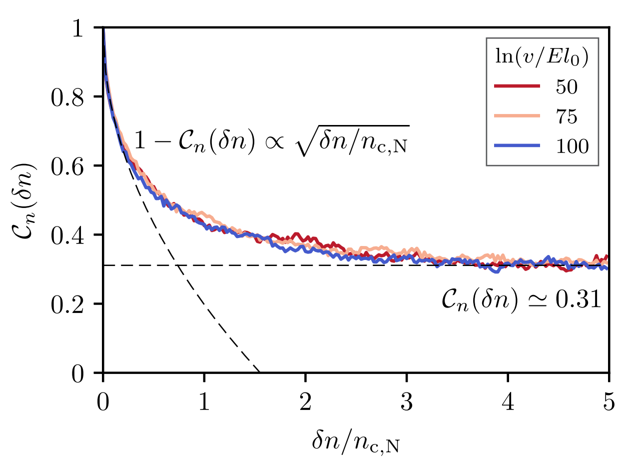

FIG. 5. Correlation function $\mathcal{C}_n(\delta n)$ of the conductances at different electron densities for $\delta n \ll n_{c,A}$. We compute $\mathcal{C}_n(\delta n)$ by simulating the evolution of the S matrix for $L = 9\times 10^4 l_0$ [see Eq. (12) and its low-energy counterpart, Eq. (S44) of Ref. [38]], and averaging the result over 5000 samples. The saturation of $\mathcal{C}_n(\delta n)$ stems from the insensitivity of the CAR amplitudes to the density variations $\delta n \ll n_{c,A}$. The curves plotted for different $\ln(v/El_0)$ coincide with each other.

In fact, $\mathcal{C}_n(\delta n)$ plotted for different energies collapses on the same curve not only at $\delta n \gg n_{c,N}$, but at all values of δn. To substantiate this observation, we find $\mathcal{C}_n(\delta n)$ analytically at $\delta n \ll n_{c,N}$. The shift $\delta k_\mu \propto \delta n$ leads to the imperfect correlation between the noises acting on the $\vec{w}$ particles at the two values of density. As a result, the particles separate in the course of their motion, $|\vec{w}_n - \vec{w}_{n+\delta n}| \sim \sqrt{\delta k_\mu \Delta x}$, where Δx is the "time" measured from the start of the last cycle [38]. Because of the separation, they may end up on opposite halves of the respective trenches leading to the deviation of $\mathcal{C}_n(\delta n)$ from unity. The motion of an individual particle happens with the diffusion coefficient $1/l_0$. It takes time $\Delta x \sim l(E)$ for the particles to spread over the respective trenches [which have lengths of the order of $\sqrt{l(E)/l_0}$]. The characteristic particle separation at that time is $\sqrt{\delta k_\mu l(E)}$. Given the characteristic particle density along a trench of $1/\sqrt{l(E)/l_0}$, the probability to find the two particles at opposite sides of the respective trench middle points is of the order of $\sqrt{\delta k_\mu l(E)}/\sqrt{l(E)/l_0} = \sqrt{\delta k_\mu l_0}$. Thus, we find $1 - \mathcal{C}_n(\delta n) \sim \sqrt{\delta n/n_{c,N}}$ with $n_{c,N} = (v/l_0)(\partial n/\partial\mu)$. The square-root behavior of $\mathcal{C}_n(\delta n)$ at $\delta n \ll n_{c,N}$ and its independence of E is in agreement with the numerical calculation.

A. Interpretation of experimental observations

Our theory offers an interpretation of the observations of Refs. [12,13]. In these experiments, a dirty superconductor provided coupling between two $\nu = 1$ counterpropagating edges. The basic assumptions of our model are consistent with this setup. Therefore, we expect the devices to be at the critical point between the topological and trivial phases, and the conductance distribution function to be symmetric, $P(G) = P(-G)$. In general, $P(G)$ can be found by sampling G in a given device by varying its electron density n. However, Refs. [12,13] reported a negative conductance weakly sensitive to the variations of n. We can explain this observation by a large correlation scale $n_{c,A}$ of CAR processes.

Since the measured conductance $|G| \ll G_Q$, we focus on the regime of strong quasiparticle absorption by vortices, $\Gamma \gg v/l_0$. In this regime, the width of $P(G)$ is of the order of $G_Q(v/\Gamma l_0)$. The conductance can be related to the probabilities p_N and p_A of the EC and CAR processes as $G = G_Q(p_N - p_A)$. In the considered perturbative regime, p_N and p_A are independent of each other, and have typical values of the order of $v/\Gamma l_0$. The former probability varies with n on the scale $n_{c,N}$, while the latter one changes on a much larger scale $n_{c,A}$. Suppose that the accessible measurement range of density n is smaller than

$n_{\mathrm{c,A}}$ but exceeds $n_{\mathrm{c,N}}$. Then, p_{A} stays approximately constant within the range, while p_{N} fluctuates with variation of n. The statistics of conductance collected in such a measurement would be $\tilde{P}(G) = \Theta(G + G_Q p_{\mathrm{A}}) \times (8\Gamma l_0/v)\exp[-(8\Gamma l_0/v)(G + G_Q p_{\mathrm{A}}/G_Q)]$. Accordingly, the probability to measure a negative conductance is $1 - \exp[-(8\Gamma l_0/v)p_{\mathrm{A}}]$. It is close to 1 if p_{A} is relatively large, $p_{\mathrm{A}} \gtrsim v/(8\Gamma l_0)$. With an assumption of an anomalously large p_{A}, this may explain the negative signal reported in Ref. [13], and even without such an assumption the data of Ref. [12]. A similar mechanism may be relevant for the observations at other integer fillings ν.

IX. CONCLUSIONS

Transport of a quantum Hall edge across a narrow superconductor is determined by the competition of CAR and EC processes. For a disordered superconductor, the amplitudes of these processes are random but are balanced statistically; see Eqs. (5) and (6). The balance automatically tunes the system to the critical point between trivial and topological phases. The charge transport at the critical point is random. At low bias $V = E/e$ (see Fig. 1 for the setup), conductance $G(E)$ is equally distributed between two quantized values, $\pm G_Q$. Which value of G is realized at a given E is determined by the disorder configuration in a segment of superconductor of length $l(E) \propto \ln^2(1/E)$. Upon changing E, $G(E)$ switches stochastically between $\pm G_Q$; see Fig. 3(a). The switchings are roughly equidistant in $\ln\,\ln(1/E)$ scale; see Eq. (19) and Fig. 3. Electron tunneling into the vortex cores breaks the quantization of G. A strong quasiparticle loss shrinks the conductance distribution $P(G)$ to a narrow interval of values around $G = 0$; see Eq. (23) and Fig. 4. $P(G)$ can be determined experimentally by collecting the statistics of the conductance fluctuations with electron density n. To achieve the representative sampling of G, the variation of n has to exceed the scale $n_{\mathrm{c,A}}$ at which the CAR amplitudes change. At smaller density variations, the conductance may appear nonergodic; see Eq. (24) and Fig. 5. Such a seemingly nonergodic behavior may be directly relevant for the data of Refs. [12,13].

Our theory identifies a challenge in engineering a topological superconductor by proximity coupling the quantum Hall edges. It demonstrates that one *cannot* reach a topological phase when using a dirty superconductor to induce the proximity effect, even when the spin-orbit interaction is strong. At the same time, it shows that the proximity-coupled edges give unprecedented access to the fundamentally interesting physics of the topological phase transition criticality. There is no need for fine-tuning of the magnetic field or the chemical potential: The strong disorder naturally tunes the device to the critical point. Looking forward, it would be interesting to extend our theory to the case of the proximity-coupled fractional quantum Hall edges.

ACKNOWLEDGMENTS

We acknowledge very useful discussions with Pavel D. Kurilovich and Gil Refael. V. D. K. also acknowledges the advice of Artem Merezhnikov on the optimization of the numerical calculations. This work is supported by NSF Grant No. DMR-2002275 (V. D. K.), and ARO Grant No. W911NF2210053 and ONR MURI Grant No. N00014-22-1-2764 (L. I. G.).

[1] C. Nayak, S. H. Simon, A. Stern, M. Freedman, and S. Das Sarma, *Non-Abelian Anyons and Topological Quantum Computation*, Rev. Mod. Phys. **80**, 1083 (2008).

[2] A. Y. Kitaev, *Unpaired Majorana Fermions in Quantum Wires*, Phys. Usp. **44**, 131 (2001).

[3] D. J. Clarke, J. Alicea, and K. Shtengel, *Exotic Non-Abelian Anyons from Conventional Fractional Quantum Hall States*, Nat. Commun. **4**, 1348 (2013).

[4] M. Cheng, *Superconducting Proximity Effect on the Edge of Fractional Topological Insulators*, Phys. Rev. B **86**, 195126 (2012).

[5] D. A. Ivanov, *Non-Abelian Statistics of Half-Quantum Vortices in p-Wave Superconductors*, Phys. Rev. Lett. **86**, 268 (2001).

[6] R. M. Lutchyn, J. D. Sau, and S. Das Sarma, *Majorana Fermions and a Topological Phase Transition in Semiconductor-Superconductor Heterostructures*, Phys. Rev. Lett. **105**, 077001 (2010).

[7] Y. Oreg, G. Refael, and F. von Oppen, *Helical Liquids and Majorana Bound States in Quantum Wires*, Phys. Rev. Lett. **105**, 177002 (2010).

[8] S. Nadj-Perge, I. K. Drozdov, B. A. Bernevig, and A. Yazdani, *Proposal for Realizing Majorana Fermions in Chains of Magnetic Atoms on a Superconductor*, Phys. Rev. B **88**, 020407(R) (2013).

[9] F. Pientka, A. Keselman, E. Berg, A. Yacoby, A. Stern, and B. I. Halperin, *Topological Superconductivity in a Planar Josephson Junction*, Phys. Rev. X **7**, 021032 (2017).

[10] D. J. Clarke, J. Alicea, and K. Shtengel, *Exotic Circuit Elements from Zero-Modes in Hybrid Superconductor–Quantum-Hall Systems*, Nat. Phys. **10**, 877 (2014).

[11] R. S. K. Mong, D. J. Clarke, J. Alicea, N. H. Lindner, P. Fendley, C. Nayak, Y. Oreg, A. Stern, E. Berg, K. Shtengel, and M. P. A. Fisher, *Universal Topological Quantum Computation from a Superconductor-Abelian Quantum Hall Heterostructure*, Phys. Rev. X **4**, 011036 (2014).

[12] G.-H. Lee, K.-F. Huang, D. K. Efetov, D. S. Wei, S. Hart, T. Taniguchi, K. Watanabe, A. Yacoby, and P. Kim, *Inducing Superconducting Correlation in Quantum Hall Edge States*, Nat. Phys. **13**, 693 (2017).

[13] O. Gül, Y. Ronen, S. Y. Lee, H. Shapourian, J. Zauberman, Y. H. Lee, K. Watanabe, T. Taniguchi, A. Vishwanath, A. Yacoby, and P. Kim, *Andreev Reflection in the Fractional Quantum Hall State*, Phys. Rev. X **12**, 021057 (2022).

[14] L. Zhao, E. G. Arnault, A. Bondarev, A. Seredinski, T. F. Q. Larson, A. W. Draelos, H. Li, K. Watanabe, T. Taniguchi,

F. Amet, H. U. Baranger, and G. Finkelstein, *Interference of Chiral Andreev Edge States*, Nat. Phys. **16**, 862 (2020).
[15] M. Hatefipour, J. J. Cuozzo, J. Kanter, W. M. Strickland, C. R. Allemang, T.-M. Lu, E. Rossi, and J. Shabani, *Induced Superconducting Pairing in Integer Quantum Hall Edge States*, Nano Lett. **22**, 6173 (2022).
[16] A. L. R. Manesco, I. M. Flór, C.-X. Liu, and A. R. Akhmerov, *Mechanisms of Andreev Reflection in Quantum Hall Graphene*, SciPost Phys. Core **5**, 045 (2022).
[17] V. D. Kurilovich, Z. M. Raines, and L. I. Glazman, *Disorder-Enabled Andreev Reflection of a Quantum Hall Edge*, Nat. Commun. **14**, 2237 (2023).
[18] N. Schiller, B. A. Katzir, A. Stern, E. Berg, N. H. Lindner, and Y. Oreg, *Superconductivity and Fermionic Dissipation in Quantum Hall Edges*, Phys. Rev. B **107**, L161105 (2023).
[19] T. H. Galambos, F. Ronetti, B. Hetényi, D. Loss, and J. Klinovaja, *Crossed Andreev Reflection in Spin-Polarized Chiral Edge States Due to the Meissner Effect*, Phys. Rev. B **106**, 075410 (2022).
[20] A. B. Michelsen, P. Recher, B. Braunecker, and T. L. Schmidt, *Supercurrent-Enabled Andreev Reflection in a Chiral Quantum Hall Edge State*, Phys. Rev. Res. **5**, 013066 (2023).
[21] Y. Tang, C. Knapp, and J. Alicea, *Vortex-Enabled Andreev Processes in Quantum Hall–Superconductor Hybrids*, Phys. Rev. B **106**, 245411 (2022).
[22] D. Beckmann, H. B. Weber, and H. v. Löhneysen, *Evidence for Crossed Andreev Reflection in Superconductor-Ferromagnet Hybrid Structures*, Phys. Rev. Lett. **93**, 197003 (2004).
[23] P. Cadden-Zimansky and V. Chandrasekhar, *Nonlocal Correlations in Normal-Metal Superconducting Systems*, Phys. Rev. Lett. **97**, 237003 (2006).
[24] P. W. Brouwer, M. Duckheim, A. Romito, and F. von Oppen, *Topological Superconducting Phases in Disordered Quantum Wires with Strong Spin-Orbit Coupling*, Phys. Rev. B **84**, 144526 (2011).
[25] O. Motrunich, K. Damle, and D. A. Huse, *Griffiths Effects and Quantum Critical Points in Dirty Superconductors without Spin-Rotation Invariance: One-Dimensional Examples*, Phys. Rev. B **63**, 224204 (2001).
[26] P. W. Brouwer, A. Furusaki, I. A. Gruzberg, and C. Mudry, *Localization and Delocalization in Dirty Superconducting Wires*, Phys. Rev. Lett. **85**, 1064 (2000).
[27] A. R. Akhmerov, J. P. Dahlhaus, F. Hassler, M. Wimmer, and C. W. J. Beenakker, *Quantized Conductance at the Majorana Phase Transition in a Disordered Superconducting Wire*, Phys. Rev. Lett. **106**, 057001 (2011).
[28] D. S. Antonenko, E. Khalaf, P. M. Ostrovsky, and M. A. Skvortsov, *Mesoscopic Conductance Fluctuations and Noise in Disordered Majorana Wires*, Phys. Rev. B **102**, 195152 (2020).
[29] V. Shivamoggi, G. Refael, and J. E. Moore, *Majorana Fermion Chain at the Quantum Spin Hall Edge*, Phys. Rev. B **82**, 041405(R) (2010).
[30] P. A. Lee, A. D. Stone, and H. Fukuyama, *Universal Conductance Fluctuations in Metals: Effects of Finite Temperature, Interactions, and Magnetic Field*, Phys. Rev. B **35**, 1039 (1987).
[31] E. Prada and F. Sols, *Entangled Electron Current through Finite Size Normal-Superconductor Tunneling Structures*, Eur. Phys. J. B **40**, 379 (2004).
[32] R. M. Lutchyn, T. D. Stanescu, and S. Das Sarma, *Momentum Relaxation in a Semiconductor Proximity-Coupled to a Disordered s-Wave Superconductor: Effect of Scattering on Topological Superconductivity*, Phys. Rev. B **85**, 140513(R) (2012).
[33] E. M. Lifshitz and L. P. Pitaevskii, *Statistical Physics* (Butterworth-Heinemann, Oxford, 1980).
[34] I. L. Aleiner and A. I. Larkin, *Divergence of Classical Trajectories and Weak Localization*, Phys. Rev. B **54**, 14423 (1996).
[35] F. W. J. Hekking and Y. V. Nazarov, *Subgap Conductivity of a Superconductor–Normal-Metal Tunnel Interface*, Phys. Rev. B **49**, 6847 (1994).
[36] A. Abrikosov and L. Gor'kov, *Spin-Orbit Interaction and the Knight Shift in Superconductors*, Sov. Phys. JETP **15**, 752 (1962), http://jetp.ras.ru/cgi-bin/e/index/e/15/4/p752?a=list.
[37] M. G. Vavilov and L. I. Glazman, *Conductance of Mesoscopic Systems with Magnetic Impurities*, Phys. Rev. B **67**, 115310 (2003).
[38] See Supplemental Material at http://link.aps.org/supplemental/10.1103/PhysRevX.13.031027 for details of the derivations of Eqs. (6), (9), and (13), a derivation of the variance of the forward-scattering phase, an additional discussion of the parametric correlations, and a derivation of the conductance distribution function valid at an arbitrary quasiparticle loss Γ.
[39] See Refs. [40,41] for a related discussion of the comparison between EC and CAR.
[40] G. Falci, D. Feinberg, and F. W. J. Hekking, *Correlated Tunneling into a Superconductor in a Multiprobe Hybrid Structure*, Europhys. Lett. **54**, 255 (2001).
[41] G. Bignon, M. Houzet, F. Pistolesi, and F. W. J. Hekking, *Current-Current Correlations in Hybrid Superconducting and Normal-Metal Multiterminal Structures*, Europhys. Lett. **67**, 110 (2004).
[42] Vortices are induced in the superconducting electrode if the magnetic field exceeds the width-dependent lower critical field $H_{c1}(d)$. For a narrow electrode $d \sim \xi$, the latter field is comparable to the upper critical one [43,44].
[43] A. Abrikosov, *On the Lower Critical Field of Thin Layers of Superconductors of the Second Group*, Sov. Phys. JETP **19**, 988 (1964), http://jetp.ras.ru/cgi-bin/e/index/e/19/4/p988?a=list.
[44] K. K. Likharev, *The Formation of a Mixed State in Planar Semiconductor Films*, Radiophys. Quantum Electron. **14**, 722 (1971).
[45] We promote the variables $\eta_{m,\alpha}(x)$ and $\vartheta_j(x)$ defined on a discrete set of elements to the continuous fields. This is why we use $\delta(x - x')$ instead of $\delta_{xx'}$.
[46] We use $G(E)$ as a shorthand notation for the differential conductance $G(V, T = 0)$ at bias $V = E/e$.
[47] P. W. Brouwer, M. Duckheim, A. Romito, and F. von Oppen, *Probability Distribution of Majorana End-State Energies in Disordered Wires*, Phys. Rev. Lett. **107**, 196804 (2011).

[48] We remind that only the condition $\lambda > 0$ arises naturally for a disordered superconductor; see the discussion around Eq. (7). It is nonetheless instructive to consider the case $\lambda < 0$ as well.

[49] The effective temperature coincides with the diffusion coefficient $1/l_0$, consistent with the Einstein relation for a Brownian particle with a unit mobility.

[50] F. J. Dyson, *The Dynamics of a Disordered Linear Chain*, Phys. Rev. **92**, 1331 (1953).

[51] D. S. Fisher, *Random Antiferromagnetic Quantum Spin Chains*, Phys. Rev. B **50**, 3799 (1994).

[52] Forward scattering phases $\vartheta_{R/L}$ are inconsequential for finding $P(G)$, so we suppress them in Eq. (22).

[53] P. A. Lee and A. D. Stone, *Universal Conductance Fluctuations in Metals*, Phys. Rev. Lett. **55**, 1622 (1985).

[54] B. L. Altshuler, *Fluctuations in the Extrinsic Conductivity of Disordered Conductors*, JETP Lett. **41**, 530 (1985), http://jetpletters.ru/ps/1470/article_22425.shtml.